

Supernova neutrino physics with a nuclear emulsion detector

G. De Lellis^{1,2}, A. Di Crescenzo^{1,2}, A. Gallo Rosso^{*3,4}, V. Gentile^{†3,4}
and F. Vissani⁴

¹*Università Federico II di Napoli, Dipartimento di Fisica,
Via Cintia 21, 80126 Napoli, Italy*

²*INFN, Sezione di Napoli, Via Cintia 21, 80126 Napoli, Italy*

³*Gran Sasso Science Institute, Viale F. Crispi 7, 67100 L'Aquila, Italy*

⁴*INFN, Laboratori Nazionali del Gran Sasso, Via G. Acitelli 22,
67100 Assergi (AQ), Italy*

Abstract

The existence of the coherent neutrino-nucleus scattering reaction requires to evaluate, for any detector devoted to WIMP searches, the irreducible background due to conventional neutrino sources and at same time, it gives a unique chance to reveal supernova neutrinos. We report here a detailed study concerning a new directional detector, based on the nuclear emulsion technology. A Likelihood Ratio test shows that, in the first years of operations and with a detector mass of several tens of tons, the observation of the supernova signal can be achieved. The determination of the distance of the supernova from the neutrinos and the observation of ^8B neutrinos are also discussed.

Introduction

It has been estimated that, at a redshift $z \simeq 0.4$, the rate of core-collapse supernovae is about 10^6 per year [1]. However, when we restrict ourselves to the subset of those that are sufficiently close to produce a detectable neutrino signal, the rate is just a few per century, see e.g. [2]. This makes the detection of neutrinos from the next galactic core-collapse supernova a once-in-a-lifetime opportunity of taking a glimpse into extreme physics, such as the formation of neutron stars (or other compact remnants), explosion of massive stars, correlation with other types of radiation, as well as standard or non-standard neutrino oscillations mechanisms [3].

Standard supernova detectors such as Super-Kamiokande [4], LVD [5] or IceCube [6] are constantly ready to reveal the next galactic supernova explosion and in case of an event they will provide us with huge data sets, although consisting mainly of electron antineutrinos. As pointed out in [7, 8], it is essential to observe other types of neutrinos, to achieve the minimal goal of measuring the total energy emitted in neutrinos with a reasonable accuracy.

*Corresponding author: andrea.gallorosso@gssi.it.

†Corresponding author: valerio.gentile@gssi.it.

More in general, in order to fully profit of the scientific occasion offered by a future galactic supernova explosion and to try and obtain a complete picture of supernova neutrino emission, it will be necessary to observe as many channels as possible, including a significant neutral-current sample. We recall that neutral-current events are free from the uncertainties that currently affect the description of neutrino oscillations.

Detectors aiming at WIMP dark matter detection have to reach high standards of purity and noise reduction, which makes them also good supernova neutrino detectors, via coherent elastic neutrino scattering on nuclei. In fact, the nuclear recoil on silver target (Ag) is the same (6 keV) if given by a WIMP with mass $m_\chi \sim 25$ GeV travelling at $v_\chi \sim 260$ km s⁻¹ or by a neutrino with energy $E_\nu \sim 17$ MeV. This consideration already illustrates that supernova neutrinos and high energy solar neutrinos are potentially detectable in suitable dark matter detectors. The other key requirements of the detectors are: a sufficient mass, a continuous operation, stability. In the absence of an external trigger, a smoking gun for the identification of supernova neutrinos is the measurement of their incoming direction. This can be implemented thanks to innovative dark matter (and neutrino) detectors based on very-fine grained (nanometric) nuclear emulsion films [9].

In this paper we have evaluated quantitatively and for the first time the possibility of detecting and identifying coherent elastic neutrino nucleus scattering with nanometric emulsion detectors exploiting directional information. We will consider the setup foreseen for the NEWSdm detector, whose nanometric nuclear emulsion films are capable to reconstruct the trajectories down to 50 nm and with an intrinsic angular resolution of about 13° [10].

1 Supernova neutrinos

Supernova neutrino fluxes are predicted by means of complex simulations affected by significant uncertainties, which limit the chances of reliably predicting the aftermath of core collapse events, and in particular, the interaction rates. The distance of the next gravitational collapse in the Milky Way can be estimated statistically by the study of the astronomical precursors and descendants of the supernovae of this type, that have all similar spatial distributions. The typical average distance is slightly more than the distance of the Galactic centre and the variance is significant; the simplest reasonable estimation (10 ± 4.5) kpc [11] is rather similar to those of other more sophisticated evaluations, such as (10.7 ± 4.9) kpc [12] or (10 ± 4) kpc from Fig. 2 of [13]. However, note that these are mean values; the mode of the distance distribution is around 8.5 kpc, i.e. the distance from the Galactic Centre [11]. Since this value is compatible within the range given in the former evaluations, in the following we will consider a supernova explosion occurring at a distance of $D = 8$ kpc which is the conventional value adopted for this type of calculations.

The formation of a neutron star requires to radiate $\mathcal{E}_B \sim 3 \times 10^{53}$ erg in neutrinos. This value is the standard one usually assumed in literature (see e.g. [14, 15, 16]). The total energy is assumed to be equally distributed among the six neutrino species:

$$\mathcal{E}_i = 0.5 \times 10^{53} \text{ erg} \quad \text{with} \quad i = \nu_e, \bar{\nu}_e, \nu_x. \quad (1)$$

The notation ν_x stands for one among the four non-electronic species: $\nu_\mu, \bar{\nu}_\mu, \nu_\tau, \bar{\nu}_\tau$. The energy equipartition is a useful working hypothesis, even if it might be true only within a factor two [17]. Mean energies are expected to follow the hierarchy $\langle E_{\nu_e} \rangle \leq \langle E_{\bar{\nu}_e} \rangle \leq \langle E_{\nu_x} \rangle$ but the debate about their ratios is still open [17]. In the following we adopt the choice proposed in Ref. [14]:

$$\langle E_{\nu_e} \rangle = 9.5 \text{ MeV}, \quad \langle E_{\bar{\nu}_e} \rangle = 12 \text{ MeV}, \quad \langle E_{\nu_x} \rangle = 15.6 \text{ MeV}. \quad (2)$$

These values are in agreement with numerical simulations and also with the experimental observations from SN 1987A [15, 16, 18].

We use time integrated fluxes (fluences) derived from the quasi-thermal parameterisation firstly proposed in Ref. [19]:¹

$$\mathcal{F}_i(E_\nu) = \frac{dF_i}{dE_\nu} = \frac{\mathcal{E}_i}{4\pi D^2} \frac{E_\nu^{\alpha_i} e^{-E_\nu/T_i}}{T_i^{\alpha_i+2} \Gamma(\alpha_i+2)} \quad \text{with } i = \nu_e, \bar{\nu}_e, \nu_x \quad (3)$$

where E_ν is the neutrino energy, $\Gamma(x)$ is the Euler gamma function and T_i is the temperature, linked to the mean energy by the relation:

$$T_i = \langle E_i \rangle / (\alpha_i + 1). \quad (4)$$

The so-called *pinching parameter* α parametrises the deviation from the thermal Maxwell-Boltzmann distribution (reproduced by $\alpha = 2$).

The fluences are expected to be described by distributions with α slightly larger but not far from 2, namely, mild deviations from the hypothesis of a thermal distribution — see Ref. [18, 7, 20, 8] for a discussion. In the following calculations, we will adopt the value

$$\alpha_i = 2.5 \quad \text{with } i = \nu_e, \bar{\nu}_e, \nu_x. \quad (5)$$

As discussed in Ref. [18], is consistent with the signal seen from SN1987A. Fluences are reported in Fig. 1 as a function of the above defined parameters.

1.1 Neutral-current coherent interaction

The differential cross-section in the solid angle Ω , describing the coherent interaction between a neutrino and a nucleus mediated by the Z^0 boson, can be written as [21]:

$$\frac{d\sigma}{d\Omega} = \frac{G_F^2}{(2\pi)^2} \frac{Q_w^2}{4} \frac{E_\nu^2 (1 + \cos\theta)^2}{[1 + (1 - \cos\theta) E_\nu/M]^3} F^2(Q) \quad (6)$$

where G_F is the Fermi constant, E_ν is the neutrino energy, θ the angle of the scattered neutrino with respect to the incoming direction, M is the nucleus mass² and Q_w is the weak charge. For a nucleus with N neutrons and Z protons its value is:

$$Q_w = N - \left(1 - 4 \sin^2 \vartheta_W\right) Z. \quad (7)$$

with ϑ_W the Weinberg angle. It depends on the transferred four-momentum Q , but for $Q \lesssim 100 \text{ MeV}$ it is almost constant and equal to [22]:

$$\sin^2 \vartheta_W \approx 0.239. \quad (8)$$

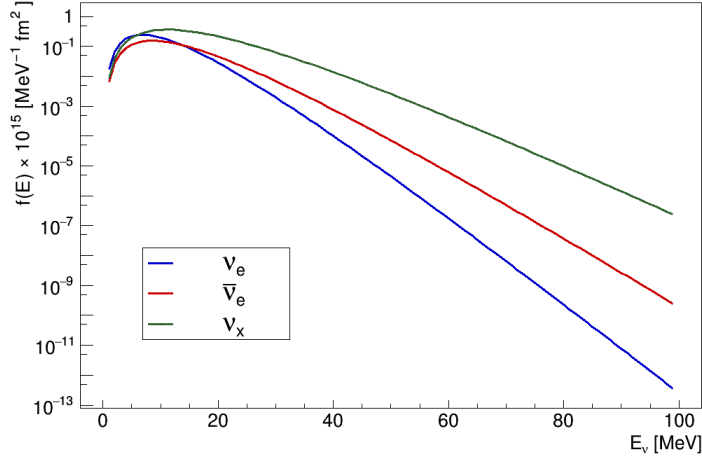


Figure 1: Fluences for the three neutrino species as defined in (3) with the parameters indicated in (1), (2) and (5).

The function $F(Q)$ is the form factor, accounting for the nucleus size, when the transferred four-momentum is nonzero. In plane-waves approximation it is the Fourier transform of the nuclear charge distribution. Following Ref. [23] and using the density given by the Helm model [24], one obtains:

$$F(Q) = \frac{3}{Q R_n} \left[\frac{\sin(Q R_n)}{(Q R_n)^2} - \frac{\cos(Q R_n)}{(Q R_n)} \right] \exp\left(-\frac{(Q s)^2}{2}\right), \quad (9)$$

where $s \approx 0.9$ fm and:

$$R_n^2(\text{fm}^2) \approx 1.5129 A^{2/3} - 1.4760 A^{1/3} + 2.5371, \quad (10)$$

with A the nucleus mass number. Combining all together, and integrating (6) over the solid angle, one obtains the expression for the energy dependent total cross-section $\sigma(E_\nu)$, shown in Fig. 2 for the target elements considered in the next sections.

Following Ref. [25], the differential rate of expected events in the nucleus recoiling energy K can be written as:

$$\frac{dN_i}{dK} = N_T \iint d\Omega dE_\nu \frac{d\sigma}{d\Omega} \mathcal{F}_i(E_\nu) \delta\left(K - \frac{Q^2}{2M}\right), \quad (11)$$

where M is the nucleus mass, N_T the number of target nuclei and δ is the Dirac delta function. Using the expression (6) and the properties of the delta function one obtains:

$$\begin{aligned} \frac{dN_i}{dK} = & N_T \frac{G_F^2 Q_w^2}{2\pi} \frac{1}{4} F^2(2MK) \int_{E_{\text{inf}}}^{\infty} dE_\nu \times \\ & \times \mathcal{F}_i(E_\nu) \left(1 + \frac{MK + KE_\nu - E_\nu^2}{(K - E_\nu) E_\nu}\right) \frac{ME_\nu^2}{(K - E_\nu)^2}, \end{aligned} \quad (12)$$

¹In the following $\hbar = c = k_B = 1$ is assumed.

²A mass independent expression is obtained by neglecting the terms order E_ν/M .

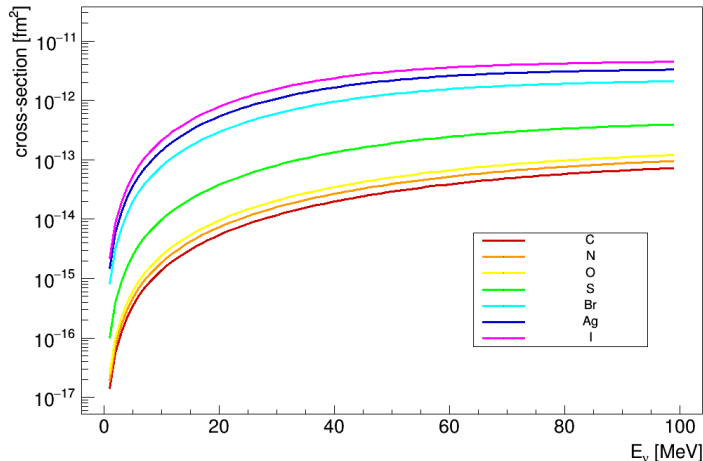


Figure 2: Energy dependent cross-section for neutral-current neutrino-nucleus interaction after integrating the differential cross-section (6) over the solid angle.

with:

$$E_{\text{inf}} = \frac{1}{2} \left(K + \sqrt{2MK + K^2} \right). \quad (13)$$

Integrating (12) over the energy from the detector threshold K_{thr} , one can obtain the number of interactions of the i -th neutrino species. Summing over all the neutrino species one obtains the total number of expected events, shown in Fig. 3 as a function of the nucleus recoil energy threshold, for a ton of active mass. The elements considered here are the same as in Fig. 2.

2 NEWSdm detector

The next generation of ton-scale detectors for dark matter search will be sensitive to neutrinos coming both from the Sun and supernova explosions. Neutrino sources lead to detectable events the current experiments due to the coherent elastic neutrino nucleus scattering (CE ν NS). This can be a source of *background*, unless these events can be tagged by means of directional sensitivity.

Measuring the direction of nuclear recoils appears to be the only strategy to go beyond the neutrino bound. On top of that, directional dark matter detectors operating during a supernova explosion can identify the *signal* due to neutrino interactions.

The NEWSdm experiment (Nuclear Emulsions for WIMP Search with directional measurement) [10] is a detector for a directional dark matter search. Nuclear emulsions are made of crystals of silver halide immersed in an organic gelatine. The passage of a charged particle through the emulsion produces along its path atomic-scale perturbations, called latent images. The chemical treatment makes Ag grains visible with an optical microscope. A track will therefore result in a sequence of aligned grains.

The NEWSdm detector consists of a bulk of new generation nuclear emulsion films called *Nano Imaging Trackers* (NIT) with nanometric size grains [26]. They are produced at

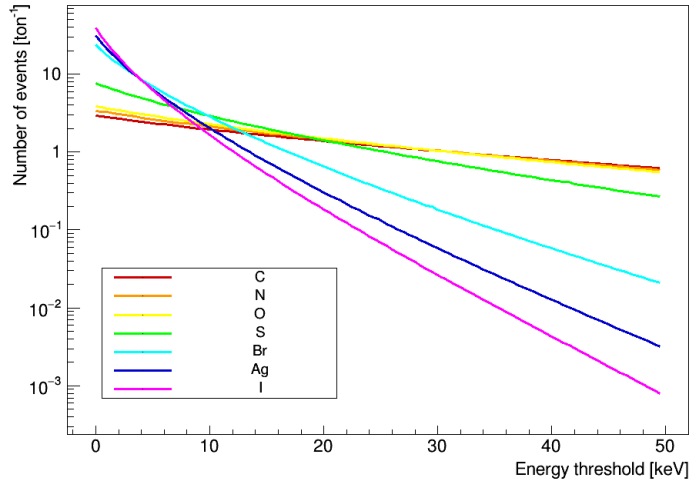


Figure 3: Total number of events of supernova neutrino induced recoils per ton of active mass, as a function of the threshold on the recoiling nucleus energy. Different colours represent different target elements.

Nagoya University in Japan where emulsions with 20 nm of diameter crystals have been already produced [9]. The reconstruction of trajectories with path lengths as short as 50 nm is possible if analysed by means of microscopes with enough resolution. The chemical composition of these emulsion films is reported in Tab. 1.

The NEWSdm experiment uses fully automated optical microscopes to perform the emulsion analysis. A 3D reconstruction with nanometric accuracy is currently feasible. Moreover, the R&D for a new scanning system is ongoing to enable the analysis of ton-scale detectors on a time scale comparable with the exposure time [27, 28, 29].

The challenging task of detecting track lengths shorter than the diffraction limit — ~ 200 nm — is achieved adopting a two-step approach: (i) candidate selection with elliptical shape analysis, (ii) candidate validation with polarised light analysis. The scanning with optical microscope cannot distinguish two grains closer than ~ 200 nm since they would appear as a single cluster, according to the Rayleigh criterion for visible light. Nevertheless, the cluster would have an elliptical shape with the major axis along the actual direction of the recoiled nucleus, unlike single grains from thermal excitation that would appear as spherical [30].

The candidate tracks selected by the elliptical shape analysis are then validated using an innovative technique which allows to overcome the intrinsic limit of the optical resolution: the polarised light analysis. The resonance effect of polarised light, occurring when nanometric metallic (silver) grains are dispersed in a dielectric medium (organic gelatine), is sensitive to the shape of nanometric grains [31]: since silver grains in the emulsions are not spherical, the resonant response depends on the polarisation of the incident light. The shortest detectable tracks are made of two grains, to be distinguished from clusters produced by a single grain.

Given the random orientation of the two grains building up the track, each grain is emphasised at different polarisation values. Taking multiple measurements over the

Element	Mass fraction	Atomic Fraction
Ag	0.44	0.10
Br	0.32	0.10
C	0.101	0.214
O	0.074	0.118
N	0.027	0.049
I	0.019	0.004
H	0.016	0.410
S	0.003	0.003
Density		3.43 g/cc

Table 1: Chemical composition of NIT emulsions.

whole polarisation range produces a displacement of the barycentre of the cluster, thus becoming sensitive to the actual presence of two grains within the cluster.

On the contrary single grains do not produce any displacement and can therefore be distinguished. Using this effect, an unprecedented accuracy better than 10 nm on the position of single grains was achieved in both (x, y) coordinates. This technique was extended to a 3D reconstruction [32].

The NEWSdm detector will be placed in the Gran Sasso Underground Laboratory, surrounded by a shield to reduce external background sources. It will be placed on an equatorial telescope in order to keep its orientation towards the Cygnus constellation fixed, where the WIMP wind is supposed to come from. The emulsion films will be placed parallel to the Galactic plane. This peculiar orientation is ideally suited for the detection of neutrinos produced by supernova explosions, since these phenomena are expected to occur in the galactic plane, where the star density is higher.

The emulsion reference frame used in this paper has the X_e and Y_e axes pointing towards the Cygnus constellation and the Galactic Centre, respectively. The Z_e axis is perpendicular to the Galactic Plane. Spherical coordinates (ϕ_e, θ_e) have been used to indicate the direction of the induced nuclear recoils: θ_e is the inclination angle from the galactic X_e - Y_e plane while ϕ_e is the angle in the galactic plane from the Cygnus direction

$$\theta_e \in \left[-\frac{\pi}{2}, \frac{\pi}{2}\right] \quad \phi_e \in (-\pi, \pi]. \quad (14)$$

Details about the reference system, the coordinate systems and their relationships are described in Appendix A.

3 Neutrinos and background sources

Simulation studies based on GEANT4 toolkit [33] have been performed to predict the interaction rate in the detector due to neutrinos emitted by a supernova and to estimate the track length and the angular distributions of the induced recoils. On the other hand, the supernova neutrino signal can be mimicked mainly by two background sources: radiogenic neutrons and solar neutrinos from ${}^8\text{B}$. Neutron induced recoils cannot be

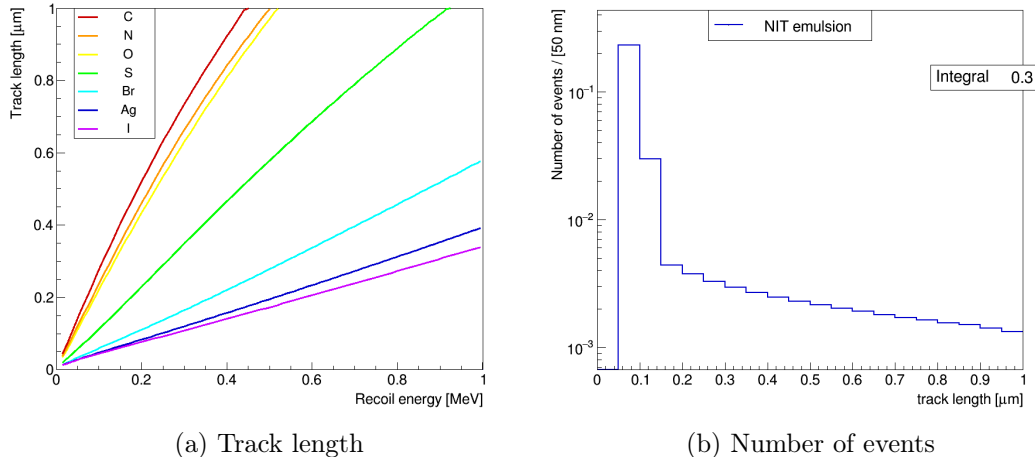


Figure 4: (a) Track length versus transferred energy for the target nuclei of NIT emulsions. Lighter nuclei can produce track lengths up to a few microns, while heavier ones only up to a few hundreds nanometers. (b) Track length distribution in NIT emulsions of supernova neutrino induced recoils in the range $[0.05, 1] \mu\text{m}$. The distribution is normalised to the number of expected events in one ton of active mass.

distinguished from the $\text{CE}\nu\text{NS}$ in the detector. Moreover, ton scale detectors for dark matter search are also sensitive to solar neutrinos.

3.1 Supernova neutrino signal

Neutrinos coming from a supernova explosion can produce tracks in NIT emulsions with lengths depending on the kinetic energy transferred to the recoiled nucleus (see Eq. 13). The number of expected events depends on the detector threshold, the exposed mass and the distance of the source from the Earth.

For nuclear emulsion detectors the energy threshold corresponds to the minimum detectable track length. The correlation between the transferred energy to the recoiled nucleus and the expected range in emulsions has been evaluated for each target element using SRIM [34]. The track length L of nuclear recoils induced by supernova neutrino scattering versus the transferred energy is reported in Fig. 4a for each target nucleus. Only energies corresponding to recoil track lengths equal or larger than 50 nm have been considered for the integral in Eq. 12. Assuming the parameters defined in Sec. 1, the total number of expected events in the whole detector is 0.30 ton^{-1} .

Distributions of $\text{CE}\nu\text{NS}$ kinematic variables have been simulated through a Monte Carlo generation. The track length distribution of the induced recoils normalized to the number of expected events is reported in Fig. 4b in the $[0.05, 1] \mu\text{m}$ range.

The scattering angle θ_{sc} is defined as the angle between the incoming neutrino direction and the one of the scattered nucleus. Its value can be obtained by the following relation:

$$\cos \theta_{sc} = \frac{E_\nu + M}{E_\nu} \sqrt{\frac{K}{2M}}, \quad (15)$$

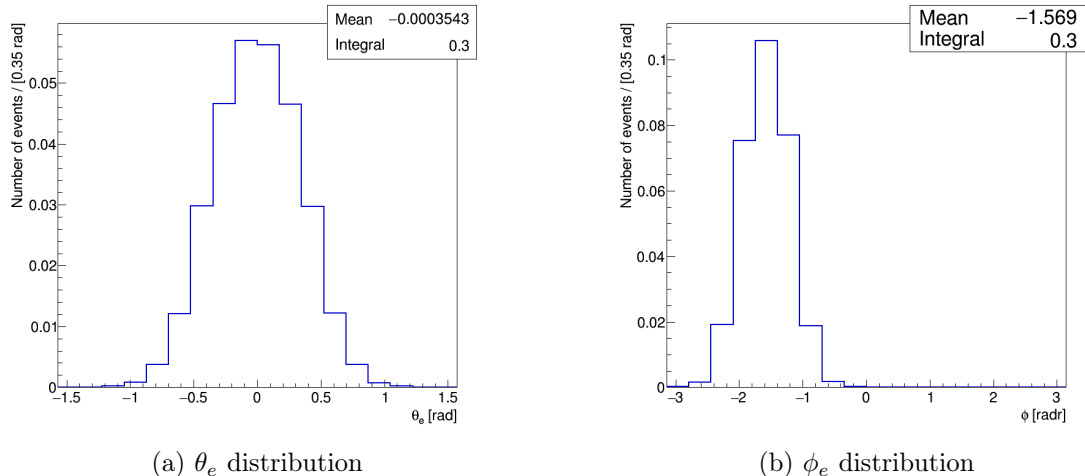


Figure 5: Distributions of the emulsion angles θ_e (a) and ϕ_e (b) of supernova neutrino induced recoils in the NEWSdm detector. The induced recoils are scattered mainly in the direction ($\theta_e = 0$) and opposite to the incoming supernova neutrino direction ($\phi_e = -\pi/2$).

where K is the transferred kinetic energy in the non-relativistic limit ($|\vec{v}_{rec}| = \sqrt{2K/M}$). Assuming a supernova explosion from the direction of the Galactic Centre, the scattering angles of neutrino induced recoils are generated and the angular distributions of θ_e and ϕ_e derived as reported in Fig. 5a and 5b (see Appendix A).

In this study it is assumed that the incoming neutrino direction points to the Galactic Centre, since it is the region where the stellar mass density is higher and therefore there is a higher probability for a supernova explosion; note that this argument is supported by the distribution of the historical records of supernova remnants and supernovas, see e.g. Ref. [35].

The θ_e angle distribution is peaked at zero since induced recoils are mostly diffused around the neutrino incoming direction; the ϕ_e angle distribution is peaked at $-\pi/2$ rad, along the negative $-Y_e$ axis corresponding to the direction opposite to the Galactic Centre.

3.2 Background sources

Background from β -rays produced in ^{14}C decays is expected to be negligible since NIT emulsions are hardly sensitive to electron recoils, in particular when cooled down to $\sim 100\text{ K}$ [36]. The replacement of gelatin with synthetic polymers is also being studied. The main background sources is therefore induced by neutrons.

Neutron-induced recoils from intrinsic contamination in NIT emulsions were recently evaluated with a GEANT4 simulation, giving a yield of ~ 1 neutron $\text{kg}^{-1}\text{y}^{-1}$ [37]. This study has also shown that the neutron-induced events can be reduced down to $0.06\text{ kg}^{-1}\text{y}^{-1}$ exploiting directionality and track length cuts. This result was obtained without any purification of the materials involved [37].

Nowadays ton-scale detectors for direct dark matter search have made the external neu-

tron background negligible using appropriate shields. For what concerns intrinsic background materials are used for ultra-low radioactivity detectors. As a result of this effort the radiogenic neutrons are typically reduced down to the level of ~ 1 neutron $\text{ton}^{-1} \text{y}^{-1}$. In this study we assume that NEWSdm will reach the same high-purity standards. The track lengths of supernova neutrino induced recoils are at least a few hundred nanometers long. For this reason, only track lengths shorter than $1 \mu\text{m}$ can be dangerous for the signal observation. The number of neutron-induced recoils with track lengths in the $[0.05, 1] \mu\text{m}$ range amounts to $\sim 0.33 \text{ton}^{-1} \text{y}^{-1}$, where fiducial volume effects have been accounted for.

3.3 Solar neutrinos from ${}^8\text{B}$

Ton-scale mass detectors are sensitive also to the recoils induced by solar neutrinos from ${}^8\text{B}$ whose energies extend up to $\sim 16 \text{MeV}$ as shown in Fig. 6. The total rate of expected events is given by

$$\frac{dN}{dt} = N_T \iint_{E_{\text{inf}}} d\Omega dE_\nu \frac{d\sigma}{d\Omega} \frac{d\Phi_\nu}{dE_\nu} \quad (16)$$

where $d\Phi_\nu/dE_\nu$ is the differential solar neutrino flux (see Fig. 6).

Note that the ${}^8\text{B}$ solar neutrino flux has been measured by SNO with neutral currents [38] and the result $\Phi_{\text{B}}^{\text{SNO}} = (5.25 \pm 0.21) \times 10^6 \text{cm}^{-2} \text{s}^{-1}$ is more precise than the theoretical predictions and it is independent upon neutrino oscillations.

The direction of incoming neutrinos from ${}^8\text{B}$ has been simulated using the projection of the Earth velocity around the Sun onto galactic axes [39]. The Earth revolution orbit is assumed to be circular. The Mollweide projection in a Galactic-like coordinate system of the induced recoils, assuming one ton per year exposure, is reported in Fig. 7 where the magenta line represents the revolution of the Earth around the Sun. The number of expected induced recoils with track lengths in the $[0.05, 1] \mu\text{m}$ range amounts to $\sim 0.18 \text{ton}^{-1} \text{y}^{-1}$. The observation of ${}^8\text{B}$ neutrinos would be relevant as a control sample.

4 Results

The expected number of nuclear recoils induced by neutrinos and neutrons is proportional to the target mass. Being the supernova explosion a transient phenomenon, the signal from supernova neutrinos does not depend on the exposure time but rather on the inverse of the squared distance D , as shown in Fig. 8 assuming a 50nm threshold in the detection of nuclear recoil tracks. On the contrary, the background from solar neutrinos and neutrons is proportional to the exposure time.

The total number of expected events depends also on the detection threshold. The potentiality of the observation of the supernova neutrinos was studied assuming a signal region ranging from 50nm to $1 \mu\text{m}$, for a detector mass of 30ton and a distance D of 8kpc . The corresponding number of expected events is:

$$N(\nu|\text{SN}) = 9.0. \quad (17)$$

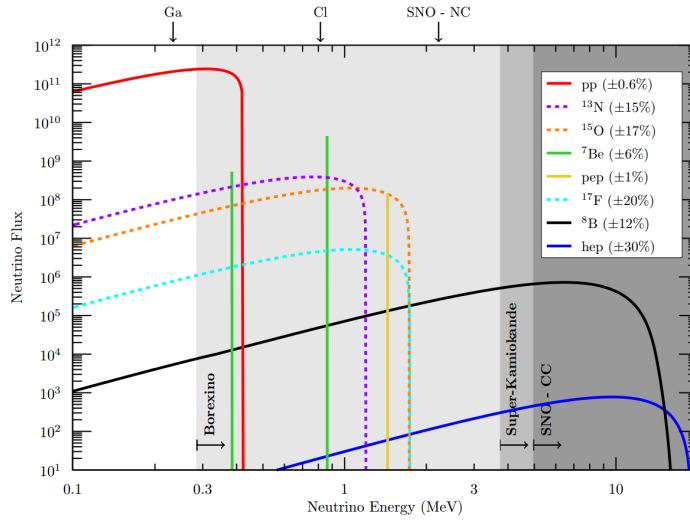


Figure 6: Solar neutrino flux $d\Phi_\nu/dE_\nu$ for each source as a function of the energy [40] along with the sensitivity regions of the various solar neutrino experiments [41].

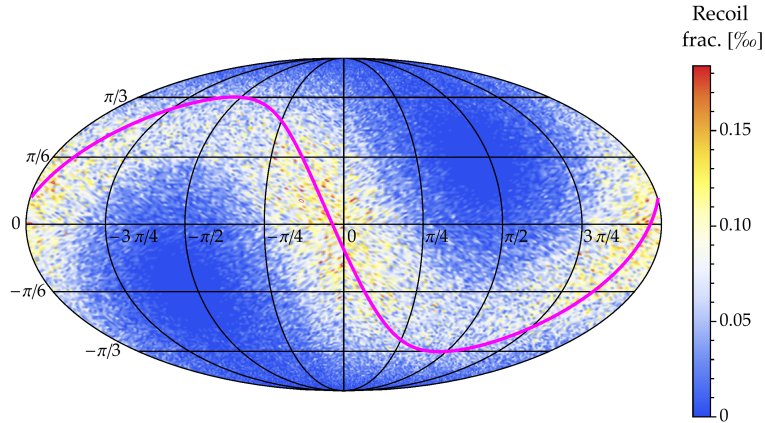


Figure 7: Mollweide projection in a Galactic-like coordinate system of the induced recoils from ^8B solar neutrinos: the latitude corresponds to θ_e while the longitude to $\phi_e - \pi/2$ (see Appendix A). The magenta line marks the neutrino arrival direction, i.e. from the Sun to the Earth.

On the other hand, the rate due to ^8B neutrinos and background neutrons n due to intrinsic contamination (IC) is:

$$N(\nu, ^8\text{B}) = 5.4 \text{ y}^{-1}; \quad (18)$$

$$N(n, \text{IC}) = 9.9 \text{ y}^{-1}. \quad (19)$$

4.1 Supernova neutrinos observation

In order to evaluate the capability of the NEWSdm detector to distinguish supernova neutrinos from background events, a Profile Likelihood [42] ratio test has been performed.

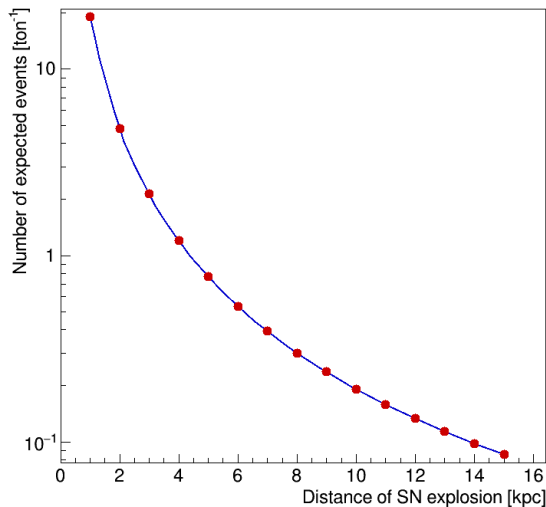


Figure 8: Number of expected events per ton of active mass as a function of the distance D of the supernova explosion.

The null hypothesis H_0 (background only) has been tested against the alternative hypothesis H_1 (signal plus background). The extended likelihood function can be written as:

$$\mathcal{L} = \frac{(\mu_s + \mu_b)^N}{N!} e^{-(\mu_s + \mu_b)} \times \prod_{i=1}^N \left(\frac{\mu_s}{\mu_s + \mu_b} \prod_j S(x_{ij}) + \frac{\mu_b}{\mu_s + \mu_b} \prod_j B(x_{ij}) \right), \quad (20)$$

where n is the total number of observed events, μ_s is the number of expected supernova neutrinos given in Eq. (17) and μ_b the expected background, obtained by multiplying the expected rates (18) and (19) by the exposure time ΔT (see e.g. Fig. 10):

$$\mu_b = \left[N(\nu, {}^8\text{B}) + N(n, \text{IC}) \right] \Delta T. \quad (21)$$

For the i -th event, the value x_{ij} is the j -th variable used in the test statistics while the functions $S(x)$ and $B(x)$ are the probability density functions (PDF) for signal and background, respectively.

A set of three variables has been used: the track length L , the ϕ_e and θ_e angles of the induced recoils. The PDFs of the three variables for supernova neutrinos, solar neutrinos from ${}^8\text{B}$ and intrinsic neutrons are reported in Fig. 9.

The significance of the test statistics for the signal plus background hypothesis (S+B) has been studied using the ROOFIT toolkit [43]. All the three above mentioned variables have been used in the Profile Likelihood function. Fig. 10a shows the mean significance as a function of the exposure time assuming 30 ton detector mass and a distance D of 8 kpc. The median expectation for the supernova neutrino signal is represented by the blue dotted line with the green (68% CL) and yellow (95% CL) solid colour regions. The shorter the exposure time the larger the significance of S+B hypothesis, since the

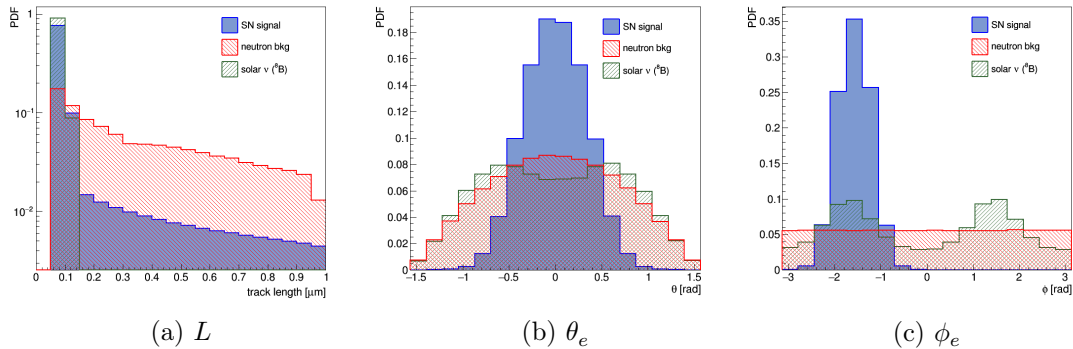


Figure 9: PDFs of recoiled nuclei, normalized to 1, induced by supernova neutrinos (blue), solar neutrinos from ^8B (green) and radiogenic neutrons (red). The track length, θ_e and ϕ_e distributions are shown in panels (a), (b) and (c), respectively.

background increases with the time while the supernova explosion is a transient event. An observation of supernova neutrinos with a confidence level larger than 3σ requires that the detector has been operated — i.e., that background events has been collected for a time shorter than 4 years.

4.2 Supernova characterisation

In addition to the signal observation, the directionality can be exploited to retrieve important information on the supernova. The likelihood function in Eq. 20 can indeed be used to derive the distance of the supernova explosion which is proportional to the inverse square root of the number of observed signal events.³ One thousand of pseudo-experiments were simulated for different distances and a fit of maximum likelihood was used to extract the number of signal events (μ_s) and therefore the measured distance D after two years of detector operation. The residual between the measured and expected distance is reported in Fig. 11 with 68% and 95% C.L. intervals. The expected median is centred at zero and the measurement is more precise for shorter distances where the signal is expected to be larger.

4.3 Solar neutrinos from ^8B as a control sample

The capability of the NEWSdm detector to identify nuclear recoils induced by solar neutrinos from ^8B has been also studied. Fig. 10b shows the mean significance as a function of the exposure for 30 ton mass detector. The median expectation for solar neutrinos from ^8B signal is represented by the blue dotted line with the green (68% CL) and yellow (95% CL) solid colour regions. The longer the exposure time the larger the significance of S+B hypothesis, since the signal-to-background ratio increases with time. After two years, an observation of the signal from ^8B solar neutrinos can be achieved with a confidence level of 3σ .

³We assume the correctness of the model exposed in Sec. 1. Note that the hypothesis on the model can be validated using the combination of different detection channels, in particular those by Super-Kamiokande and Hyper-Kamiokande [8, 7].

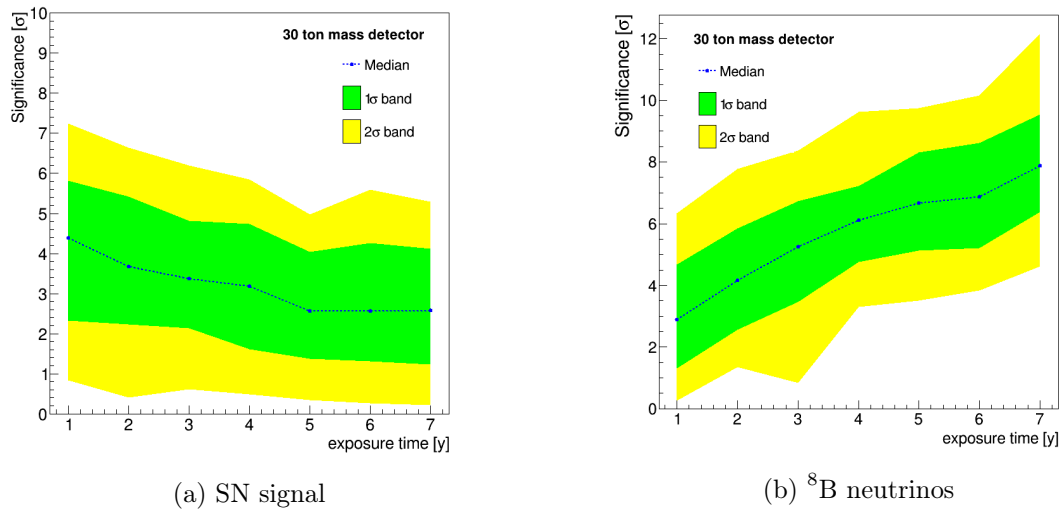


Figure 10: Mean significance as a function of the exposure time for a 30 ton mass detector (blue dotted line), for the supernova neutrino signal (a) and the ${}^8\text{B}$ neutrinos (b). The green and yellow solid colour regions show the confidence levels at 68% and 95% respectively.

Conclusions

The next generation of ton-scale detectors for dark matter searches will be sensitive to different neutrino sources like solar neutrinos from boron and neutrinos coming from a supernova explosion. Coherent elastic neutrino-nucleus scattering events are very intriguing to observe for a dark matter detector, however they can also represent a serious source of background events, unless directional information can be exploited. The capability of identifying neutral current interactions of neutrinos originated by a supernova explosion has been studied using a directional detector based on nuclear emulsions with nanometric crystals. The NEWSdm experiment uses emulsion films produced at Nagoya University made of silver halide crystals with nanometric size which make it possible to reconstruct track lengths down to 50 nm when readout with appropriate optical microscopes. Assuming the emission parameters from numerical simulations, the expected number of supernova neutrino induced recoils with path lengths ranging from 50 nm to 1 μm is about 0.30 ton^{-1} for a nominal supernova signal as defined in Sec. 1. The track length and the angular distributions have been predicted through a toy Monte Carlo and a Likelihood Ratio test has been performed to discriminate the signal from the background sources represented by the intrinsic neutrons and solar neutrinos from boron. The observation of neutrinos from a supernova exploded at 8 kpc can be obtained with a 30 ton detector only in the first few years of operation: as an example, if the supernova will explode within four years, a 3σ signal can be achieved. In this scenario, the distance of the supernova explosion from the Earth can be determined and the expected precision increases strongly for smaller distances. A Likelihood Ratio test has been also performed to discriminate recoils induced by ${}^8\text{B}$ solar neutrinos from neutron induced recoils for a control sample. A significance larger than 3σ CL is obtained with an exposure larger

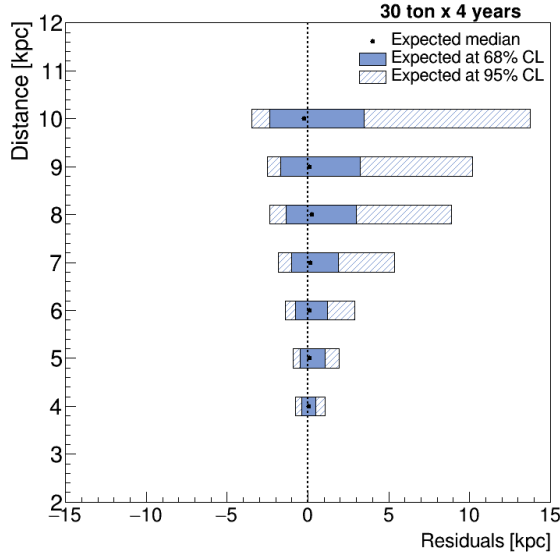


Figure 11: Residuals between the measured and expected distance.

than two years for a detector of 30 ton.

A Coordinate transformations

The calculation described in this paper make necessary coping with different coordinate systems, especially when considering the modulation rate of solar neutrinos. In order to make this tricky point as clear as possible, the relation between these systems are described in the following.

A.1 Coordinate systems

In this paper they have been adopted three main (polar) reference frames reported graphically in Fig. 12.

Scattering frame: this is the reference system where the interaction between the incident particle and the target is described — see Fig. 12a. The origin is placed in the interaction point. A unit vector in this system is identified by the scattering angles (θ_{sc}, ϕ_{sc}) where θ_{sc} is the angle between the recoiled nucleus and the direction of the incident particle, and varies in the range $[0, \pi]$. The angle ϕ_{sc} does not depend on the interaction and varies uniformly in $[0, 2\pi)$.

Standard galactic frame: this is the standard galactic reference system, with the Sun at the origin (Fig. 12b). The X_g axis points toward the Galactic Centre, the Y_g axis points in the direction of the solar system motion (Cygnus constellation) and the Z_g axis is orthogonal to the galactic X_g - Y_g plane in such a manner to keep the right-handed coordinated (North Galactic Pole). A unit vector in this coordinate system

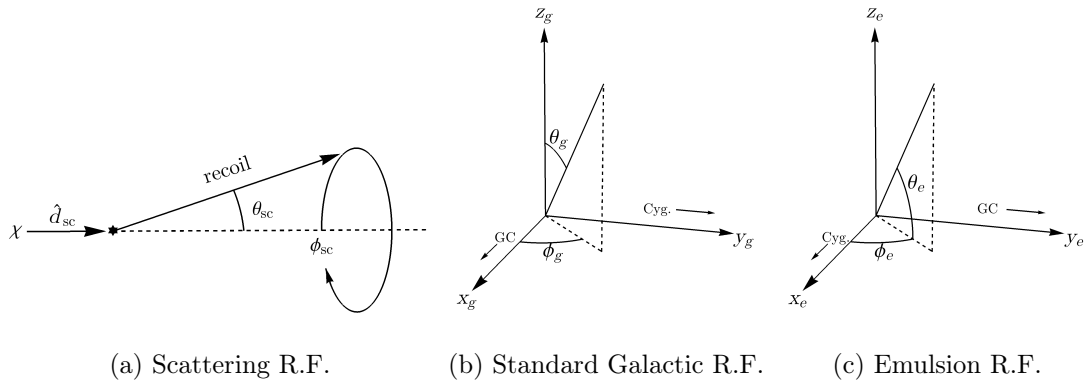


Figure 12: Reference frames used in this paper. The interaction reference frame is described in (a). In this frame, the particle χ — travelling in the \hat{d}_{sc} direction — hits a nucleus in the origin, marked by the star, generating a "recoil cone" described by the angles (θ_{sc}, ϕ_{sc}) . The systems (b) and (c) are both galactic reference frames with the sun in the origin.

is described by the polar angles (θ_g, ϕ_g) as $\hat{u}_g = (\cos \phi_g \sin \theta_g, \sin \phi_g \sin \theta_g, \cos \theta_g)$, where $\theta_g \in [0, \pi]$ and $\phi_g \in [0, 2\pi)$.

Emulsion frame: this is the NEWS-dm emulsion (galactic) reference frame, with the Sun in the origin (Fig. 12c). The X_e and Y_e axes point toward the Cygnus constellation and the Galactic Centre, respectively: the X and Y axes between the Emulsion and the standard system are swapped. As a consequence the Z_e axis points in the opposite direction of Z_g . A unit vector in this coordinate system is described by the emulsion angles (θ_e, ϕ_e) . As a convention, the θ_e angles measures the angular distance from the galactic X_e - Y_e plane and thus varies from $-\pi/2$ to $\pi/2$. The ϕ_e angle describes the angular distance from the X_e axis and varies in the range $(-\pi, \pi]$.

The procedure followed in this paper starts from the (θ_{sc}, ϕ_{sc}) distributions of the recoiling nuclei in the scattering frame which are then translated into the observed (θ_e, ϕ_e) distributions in the emulsion reference frame. Therefore, a coordinate transformation from the unit vector \hat{u}_{sc} describing the recoiling direction to the unit vector \hat{u}_e is performed. Since the latter depends on the galactic direction of the source, two different cases have been taken into account. The first one concerns neutrinos coming from a supernova explosion and is described in Sec. A.2. The second one, discussed in Sec. A.3, regards neutrinos coming from the sun. This case is more complex since it takes dynamical transformations depending on the time of the year, because of the motion of the earth around the Sun.

A.2 Supernova neutrinos

According to the galactic distribution of pre-supernova object [11], the next supernova is expected to happen not too far from the Galactic Centre. Since the emulsion frame has its Y_e axis pointed toward the Galactic Centre, the supernova neutrino signal would arrive from $+Y_e$ scattering towards $-Y_e$.

The coordinate relations between the scattering reference frame and the emulsion one are obtained considering the recoil cone reported in Fig. 12a with its axis \hat{d}_{sc} along the $-Y_e$ axis and its vertex in the origin, i.e. the detection point. The Cartesian components of the unit vector \hat{u}_e are therefore extracted as follows:

$$\hat{u}_e = \begin{cases} x_e &= \sin \theta_{sc} \cos \phi_{sc} \\ y_e &= -\cos \theta_{sc} \\ z_e &= \sin \theta_{sc} \sin \phi_{sc}, \end{cases} \quad (22)$$

where the ϕ_{sc} angle lies on the X_e - Z_e plane and starts from the X_e axis. The Cartesian coordinates in Eq. (22) are then used to obtain the (θ_e, ϕ_e) angles:

$$\phi_e = \begin{cases} \tan^{-1}(y_e/x_e) & \text{if } x_e > 0 \\ \tan^{-1}(y_e/x_e) + \pi & \text{if } y_e \geq 0 \\ \tan^{-1}(y_e/x_e) - \pi & \text{if } y_e < 0 \end{cases} \quad \text{if } x_e < 0 \quad (23)$$

$$\left. \begin{cases} \pi/2 & \text{if } y_e > 0 \\ -\pi/2 & \text{if } y_e < 0 \end{cases} \right\} \quad \text{if } x_e = 0$$

$$\theta_e = \begin{cases} [1 - \text{sig}(z_e) \cdot 1] \pi/2 & \text{if } x_e = y_e = 0 \\ \tan^{-1}\left(z_e/\sqrt{x_e^2 + y_e^2}\right) & \text{otherwise} \end{cases} \quad (24)$$

where $\text{sig}z_e$ is the sign of the z_e coordinate. The previous definitions preserve the range of $\theta_e \in [-\pi/2, \pi/2]$ and $\phi_e \in (-\pi, \pi]$.⁴ Inserting the explicit expression of the coordinates (22) in (23) and (24) the coordinate functions $\theta_e(\theta_{sc}, \phi_{sc})$ and $\phi_e(\theta_{sc}, \phi_{sc})$ that perform the coordinate changes, are obtained. According to (22), ϕ_{sc} ranges in the X_e - Z_e plane starting from the X_e axis. The (θ_e, ϕ_e) angles are defined as follows:

$$\phi_e = \begin{cases} F(\theta_{sc}, \phi_{sc}) & \text{if } \theta_{sc} \neq 0, \pi \\ F(\theta_{sc}, \phi_{sc}) - \pi & \text{if } 0 < \theta_{sc} < \pi/2 \\ F(\theta_{sc}, \phi_{sc}) + \pi & \text{if } \pi/2 \leq \theta_{sc} < \pi \end{cases} \quad \text{and} \quad \begin{cases} 0 \leq \phi_{sc} < \pi/2 \\ \text{or } \phi_{sc} > 3\pi/2 \end{cases} \quad (25)$$

$$\text{and} \quad \pi/2 < \phi_{sc} < 3\pi/2$$

$$\theta_e = \tan^{-1}\left(\sin \phi_{sc} / \sqrt{\cos^2 \phi_{sc} + \cot^2 \theta_{sc}}\right), \quad (26)$$

where for $\phi_{sc} = \pi/2, 3\pi/2$ (and $\theta_{sc} = \pi/2$) limit may be applied.

A.3 Solar neutrinos

In the case of neutrinos coming from the Sun the axis \hat{d}_{sc} (see Fig. 12a) must point, time by time, the direction from the source to the detector. Since the Earth moves around the Sun, a parametric function $f(t; \theta_{sc}, \phi_{sc})$ of the time-like parameter t is needed to reproduce the Earth's orbit when $\theta_{sc} = 0$ and $t \in [0, 2\pi)$.⁵

⁴It requires that ϕ_e is in principle undefined for $x_e = y_e = 0$.

⁵In order to keep the formulas as simple as possible, a-dimensional quantities are considered in the following.

Assuming the Earth orbit as a perfect circle with the centre in the Sun, Ref. [44] has been followed. At order zero, the Earth's orbit in standard galactic coordinates can be expressed as:

$$\hat{r}_i = \cos b_i \cos(t - \ell_i) \quad \text{with} \quad i = x_g, y_g, z_g, \quad (27)$$

where $t \in [0, 2\pi)$ is the parameter describing the orbit over one year. The parameters (b_i, ℓ_i) needed to describe the axes of the heliocentric ecliptic rectangular coordinate system in the galactic one — see Ref. [44] — are the following:

$$\begin{aligned} (b_{x,g}, \lambda_{x,g}) &= (5^\circ.536, 266^\circ.840) \\ (b_{y,g}, \lambda_{y,g}) &= (-59^\circ.574, 347^\circ.340) \quad \text{with} \quad \lambda_i = \ell_i - 180^\circ. \\ (b_{z,g}, \lambda_{z,g}) &= (-29^\circ.811, 180^\circ.023) \end{aligned} \quad (28)$$

Let us start with the \hat{d}_{sc} axis placed along the X axis of a reference frame defined in such a way that the Earth's orbit lies on the X - Y plane:

$$\hat{d}_{sc} = (1, 0, 0). \quad (29)$$

Since the versor \hat{d}_{sc} must rotate according to the annual Earth motion, a time-like parameter α that describes its rotation along the Z -axis has been introduced:

$$\hat{d}_1(\alpha) = \mathcal{R}_z(\alpha)\hat{d}_{sc} = \begin{pmatrix} \cos \alpha & -\sin \alpha & 0 \\ \sin \alpha & \cos \alpha & 0 \\ 0 & 0 & 1 \end{pmatrix} \begin{pmatrix} 1 \\ 0 \\ 0 \end{pmatrix}, \quad (30)$$

where \mathcal{R}_z is the active rotation matrix along the Z axis.

In order to reproduce the Earth motion in galactic coordinates (27), the first step is to tilt the \hat{d}_1 orbit by means of a clockwise rotation along the X axis of an angle β , according the Eq. (27). Therefore, the passive $\mathcal{R}_x^t(\beta)$ rotation matrix to the versor $\hat{d}_1(\alpha)$ defined in Eq. (30) is applied:

$$\hat{d}_2(\beta, \alpha) = \mathcal{R}_x^t(\beta)\hat{d}_1(\alpha) = \begin{pmatrix} 1 & 0 & 0 \\ 0 & \cos \beta & \sin \beta \\ 0 & -\sin \beta & \cos \beta \end{pmatrix} \begin{pmatrix} \cos \alpha & -\sin \alpha & 0 \\ \sin \alpha & \cos \alpha & 0 \\ 0 & 0 & 1 \end{pmatrix} \begin{pmatrix} 1 \\ 0 \\ 0 \end{pmatrix}. \quad (31)$$

According the Eq. (31), the intersection line between the X - Y plane and the tilted \hat{d}_2 orbit coincides with the X axis. On the other hand, from Eq. (27) the coordinates (x_g, y_g) with $z_g = 0$ are:

$$z_g = 0 \Leftrightarrow t = l_z \pm \frac{\pi}{2} \quad \Leftrightarrow \quad \begin{cases} x_g = \cos b_x \cos(l_z - l_x \pm \pi/2) & \equiv \pm x_{\text{int}} \\ y_g = \cos b_y \cos(l_z - l_y \pm \pi/2) & \equiv \pm y_{\text{int}} \end{cases} \quad (32)$$

and the azimuth position ϕ_g of the intersection point is:

$$\phi_g = \arctan\left(\frac{y_{\text{int}}}{x_{\text{int}}}\right) = 0.111419 \equiv \phi_{\text{int}}. \quad (33)$$

Therefore, to reproduce the orbit in Eq. (27) the versor $\hat{d}_2(\beta, \alpha)$ is rotated by an angle $\gamma = \phi_{\text{int}}$ along the Z axis:

$$\begin{aligned}\hat{d}_3(\gamma, \beta, \alpha) &= \mathcal{R}_z(\gamma)\hat{d}_2(\beta, \alpha) \\ &= \begin{pmatrix} \cos \gamma & -\sin \gamma & 0 \\ \sin \gamma & \cos \gamma & 0 \\ 0 & 0 & 1 \end{pmatrix} \begin{pmatrix} 1 & 0 & 0 \\ 0 & \cos \beta & \sin \beta \\ 0 & -\sin \beta & \cos \beta \end{pmatrix} \begin{pmatrix} \cos \alpha & -\sin \alpha & 0 \\ \sin \alpha & \cos \alpha & 0 \\ 0 & 0 & 1 \end{pmatrix} \begin{pmatrix} 1 \\ 0 \\ 0 \end{pmatrix}.\end{aligned}\quad (34)$$

Performing the matrix product the z -component of $\hat{d}_3(\gamma, \beta, \alpha)$ can be obtained as follows:

$$\hat{d}_{3,z}(\gamma, \beta, \alpha) = -\sin \alpha \sin \beta. \quad (35)$$

It corresponds to the third component of \hat{r} in Eq. (27) if one identifies:

$$\alpha \equiv t - \lambda_z + \frac{\pi}{2} \quad \text{and} \quad \beta \equiv \frac{\pi}{2} + b_z. \quad (36)$$

Finally, the \hat{d}_{sc} axis can be replaced with a generic scattering versor \hat{u}_{sc} . Since an initial values of \hat{d}_{sc} has been assumed along the x -axis, a possible parameterisation could be:

$$\hat{u}_{sc} = (\cos \theta_{sc}, \sin \theta_{sc} \cos \phi_{sc}, \sin \theta_{sc} \sin \phi_{sc}). \quad (37)$$

The final expression is:

$$\hat{u}_g(\theta_{sc}, \phi_{sc}; \alpha, \beta, \gamma) = \mathcal{R}_z(\gamma)\mathcal{R}_x^t(\beta)\mathcal{R}_z(\alpha)\hat{u}_{sc}(\theta_{sc}, \phi_{sc}), \quad (38)$$

or:

$$\hat{u}_g = \begin{pmatrix} \cos \gamma & -\sin \gamma & 0 \\ \sin \gamma & \cos \gamma & 0 \\ 0 & 0 & 1 \end{pmatrix} \begin{pmatrix} 1 & 0 & 0 \\ 0 & \cos \beta & \sin \beta \\ 0 & -\sin \beta & \cos \beta \end{pmatrix} \begin{pmatrix} \cos \alpha & -\sin \alpha & 0 \\ \sin \alpha & \cos \alpha & 0 \\ 0 & 0 & 1 \end{pmatrix} \begin{pmatrix} \cos \theta_{sc} \\ \sin \theta_{sc} \cos \phi_{sc} \\ \sin \theta_{sc} \sin \phi_{sc} \end{pmatrix}. \quad (39)$$

The passage from the standard galactic reference frame to the emulsion one is straightforward:

$$\hat{u}_e = (x_e, y_e, z_e) = (y_g, x_g, -z_g) \quad (40)$$

and starting from the Cartesian components x_e, y_e, z_e the polar angles (θ_e, ϕ_e) can be derived using the Eq. (23) and (24).

References

- [1] H.E. Jorgensen et al. “Evolution of Supernova Explosion Rates in the Universe”. In: *The Astrophysical Journal* 486 (1997), pp. 110–116.
- [2] F. Vissani and A. Boeltzig. “Supernova Neutrinos: Risks and Opportunities”. In: *PoS NEUTEL2015* (2015), p. 008.
- [3] M. C. Volpe. “Neutrino Astrophysics”. In: *Acta Phys. Polon. Supp.* 9 (2016), p. 769. DOI: 10.5506/APhysPolBSupp.9.769. arXiv: 1609.06747 [astro-ph.HE].
- [4] Y. Fukuda et al. “The Super-Kamiokande detector”. In: *Nucl. Instrum. Meth.* A501 (2003), pp. 418–462. DOI: 10.1016/S0168-9002(03)00425-X.

- [5] N. Y. Agafonova et al. “Implication for the Core-collapse Supernova Rate From 21 Years of Data of the Large Volume Detector”. In: *Astrophys. J.* 802.1 (2015), p. 47. DOI: 10.1088/0004-637X/802/1/47. arXiv: 1411.1709 [astro-ph.HE].
- [6] R. Bruijn. “Supernova Detection in IceCube: Status and Future”. In: *Nucl. Phys. Proc. Suppl.* 237-238 (2013), pp. 94–97. DOI: 10.1016/j.nuclphysbps.2013.04.065. arXiv: 1302.2040 [astro-ph.IM].
- [7] A. Gallo Rosso, F. Vissani, and M. C. Volpe. “Measuring the neutron star compactness and binding energy with supernova neutrinos”. In: *JCAP* 1711.11 (2017), p. 036. DOI: 10.1088/1475-7516/2017/11/036. arXiv: 1708.00760 [hep-ph].
- [8] Andrea Gallo Rosso, Francesco Vissani, and Maria Cristina Volpe. “What can we learn on supernova neutrino spectra with water Cherenkov detectors?” In: *JCAP* 1804.04 (2018), p. 040. DOI: 10.1088/1475-7516/2018/04/040. arXiv: 1712.05584 [hep-ph].
- [9] T. Asada et al. “The development of a super-fine-grained nuclear emulsion”. In: *PTEP* 2017.6 (2017), 063H01. DOI: 10.1093/ptep/ptx076. arXiv: 1705.05014 [physics.ins-det].
- [10] A. Aleksandrov et al. “NEWS: Nuclear Emulsions for WIMP Search”. In: (2016). arXiv: 1604.04199 [astro-ph.IM].
- [11] M. L. Costantini, A. Ianni, and F. Vissani. “The interest in neutrinos from core collapse supernovae”. In: *Nucl. Phys. Proc. Suppl.* 139 (2005), pp. 27–32. DOI: 10.1016/j.nuclphysbps.2004.11.209.
- [12] A. Mirizzi, G. G. Raffelt, and P. D. Serpico. “Earth matter effects in supernova neutrinos: Optimal detector locations”. In: *JCAP* 0605 (2006), p. 012. DOI: 10.1088/1475-7516/2006/05/012. arXiv: astro-ph/0604300 [astro-ph].
- [13] S. M. Adams et al. “Observing the Next Galactic Supernova”. In: *Astrophys. J.* 778 (2013), p. 164. DOI: 10.1088/0004-637X/778/2/164. arXiv: 1306.0559 [astro-ph.HE].
- [14] C. Lujan-Peschard, G. Pagliaroli, and F. Vissani. “Spectrum of Supernova Neutrinos in Ultra-pure Scintillators”. In: *JCAP* 1407 (2014), p. 051. DOI: 10.1088/1475-7516/2014/07/051. arXiv: 1402.6953 [astro-ph.SR].
- [15] Thomas J. Loredo and Donald Q. Lamb. “Bayesian analysis of neutrinos observed from supernova SN 1987A”. In: *Phys. Rev. D* 65 (6 Feb. 2002), p. 063002. DOI: 10.1103/PhysRevD.65.063002.
- [16] G. Pagliaroli et al. “Improved analysis of SN1987A antineutrino events”. In: *Astropart. Phys.* 31 (2009), pp. 163–176. DOI: 10.1016/j.astropartphys.2008.12.010. arXiv: 0810.0466 [astro-ph].
- [17] Georg G. Raffelt. “Supernova neutrino oscillations”. In: *Phys. Scripta* T121 (2005), pp. 102–105. DOI: 10.1088/0031-8949/2005/T121/014. arXiv: hep-ph/0501049 [hep-ph].
- [18] F. Vissani. “Comparative analysis of SN1987A antineutrino fluence”. In: *J. Phys.* G42 (2015), p. 013001. DOI: 10.1088/0954-3899/42/1/013001. arXiv: 1409.4710 [astro-ph.HE].

- [19] M. Th. Keil, G. G. Raffelt, and H. T. Janka. “Monte Carlo study of supernova neutrino spectra formation”. In: *Astrophys. J.* 590 (2003), pp. 971–991. DOI: 10.1086/375130. arXiv: astro-ph/0208035 [astro-ph].
- [20] I. Tamborra et al. “High-resolution supernova neutrino spectra represented by a simple fit”. In: *Phys. Rev. D* 86 (2012), p. 125031. DOI: 10.1103/PhysRevD.86.125031. arXiv: 1211.3920 [astro-ph.SR].
- [21] D. Z. Freedman. “Coherent neutrino nucleus scattering as a probe of the weak neutral current”. In: *Phys. Rev. D* 9 (1974), pp. 1389–1392. DOI: 10.1103/PhysRevD.9.1389.
- [22] J. Erler and Michael J. Ramsey-Musolf. “The Weak mixing angle at low energies”. In: *Phys. Rev. D* 72 (2005), p. 073003. DOI: 10.1103/PhysRevD.72.073003. arXiv: hep-ph/0409169 [hep-ph].
- [23] J.D. Lewin and P.F. Smith. “Review of mathematics, numerical factors, and corrections for dark matter experiments based on elastic nuclear recoil”. In: *Astropart.Phys.* 6 (1996), pp. 87–112. DOI: 10.1016/S0927-6505(96)00047-3.
- [24] Richard H. Helm. “Inelastic and Elastic Scattering of 187 – Mev Electrons from Selected Even-Even Nuclei”. In: *Phys. Rev.* 104 (5 Dec. 1956), pp. 1466–1475. DOI: 10.1103/PhysRev.104.1466. URL: <http://link.aps.org/doi/10.1103/PhysRev.104.1466>.
- [25] M. Biassoni and C. Martinez. “Study of supernova ν -nucleus coherent scattering interactions”. In: *Astroparticle Physics* 36.1 (2012), pp. 151–155. ISSN: 0927-6505. DOI: <http://dx.doi.org/10.1016/j.astropartphys.2012.05.009>. URL: <http://www.sciencedirect.com/science/article/pii/S0927650512001132>.
- [26] M. Natsume et al. “Low-velocity ion tracks in fine grain emulsion”. In: *Nucl. Instrum. Meth.* A575 (2007), pp. 439–443. DOI: 10.1016/j.nima.2007.02.109.
- [27] A. Alexandrov et al. “A new fast scanning system for the measurement of large angle tracks in nuclear emulsions”. In: *JINST* 10.11 (2015), P11006. DOI: 10.1088/1748-0221/10/11/P11006.
- [28] A. Alexandrov et al. “A new generation scanning system for the high-speed analysis of nuclear emulsions”. In: *JINST* 11.06 (2016), P06002. DOI: 10.1088/1748-0221/11/06/P06002.
- [29] Andrey Alexandrov et al. “The Continuous Motion Technique for a New Generation of Scanning Systems”. In: *Sci. Rep.* 7.1 (2017), p. 7310. DOI: 10.1038/s41598-017-07869-3.
- [30] M. Kimura and T. Naka. “Submicron track readout in fine-grained nuclear emulsions using optical microscopy”. In: *Nuclear Instruments and Methods in Physics Research Section A: Accelerators, Spectrometers, Detectors and Associated Equipment* 680 (2012), pp. 12–17. ISSN: 0168-9002. DOI: <http://dx.doi.org/10.1016/j.nima.2012.04.010>. URL: <http://www.sciencedirect.com/science/article/pii/S0168900212003622>.
- [31] H. Tamaru et al. “Resonant light scattering from individual Ag nanoparticles and particle pairs”. In: *Applied Physics Letters* 80.10 (2002), pp. 1826–1828. DOI: 10.1063/1.1461072.

- [32] A. Alexandrov et al. *Patent for 3D nanometric readout (N. 102016000132813) IT*. 2016.
- [33] S. Agostinelli et al. “GEANT4: A Simulation toolkit”. In: *Nucl. Instrum. Meth.* A506 (2003), pp. 250–303. DOI: 10.1016/S0168-9002(03)01368-8.
- [34] J. F. Ziegler, M. D. Ziegler, and J. P. Biersack. “SRIM - The stopping and range of ions in matter (2010)”. In: *Nuclear Instruments and Methods in Physics Research B* 268 (June 2010), pp. 1818–1823. DOI: 10.1016/j.nimb.2010.02.091.
- [35] D.H. Clark and F.R. Stephenson. *The Historical Supernovae*. Pergamon international library of science, technology, engineering and social studies. Pergamon Press, 1977. ISBN: 9780080209142. URL: <https://books.google.it/books?id=XseDrgEACAAJ>.
- [36] M. Kimura et al. “WIMP tracking with cryogenic nuclear emulsion”. In: *Nucl. Instrum. Meth.* A845 (2017), pp. 373–377. DOI: 10.1016/j.nima.2016.06.052.
- [37] A. Alexandrov et al. “Intrinsic neutron background of nuclear emulsions for directional Dark Matter searches”. In: *Astropart. Phys.* 80 (2016), pp. 16–21. DOI: 10.1016/j.astropartphys.2016.03.003. arXiv: 1507.03532 [astro-ph.IM].
- [38] A. Bellerive et al. “The Sudbury Neutrino Observatory”. In: *Nucl. Phys.* B908 (2016), pp. 30–51. DOI: 10.1016/j.nuclphysb.2016.04.035. arXiv: 1602.02469 [nucl-ex].
- [39] Christopher McCabe. “The Earth’s velocity for direct detection experiments”. In: *JCAP* 1402 (2014), p. 027. DOI: 10.1088/1475-7516/2014/02/027. arXiv: 1312.1355 [astro-ph.CO].
- [40] N. Vinyoles et al. “A New Generation of Standard Solar Models”. In: *The Astrophysical Journal* 835.2 (2017), p. 202. URL: <http://stacks.iop.org/0004-637X/835/i=2/a=202>.
- [41] A. Gallo Rosso et al. “Introduction to neutrino Astronomy”. In: *Proceedings of 4th Azarquiel School, Portopalo di Capo Passero, Syracuse Italia*. 2017.
- [42] G. Cowan et al. “Asymptotic formulae for likelihood-based tests of new physics”. In: *Eur. Phys. J.* C71 (2011). [Erratum: *Eur. Phys. J.*C73,2501(2013)], p. 1554. DOI: 10.1140/epjc/s10052-011-1554-0, 10.1140/epjc/s10052-013-2501-z. arXiv: 1007.1727 [physics.data-an].
- [43] W. Verkerke and D. P. Kirkby. “The RooFit toolkit for data modeling”. In: *eConf* C0303241 (2003), MOLT007. arXiv: physics/0306116 [physics].
- [44] C. McCabe. “The Earth’s velocity for direct detection experiments”. In: *JCAP* 1402 (2014), p. 027. DOI: 10.1088/1475-7516/2014/02/027. arXiv: 1312.1355 [astro-ph.CO].